Tractor beams in the Rayleigh limit

Aaron Yevick, David B. Ruffner, and David G. Grier

Phys. Rev. A **93**, 043807 — Published 5 April 2016

DOI: 10.1103/PhysRevA.93.043807

Tractor Beams in the Rayleigh Limit

Aaron Yevick, David B. Ruffner, and David G. Grier
Department of Physics and Center for Soft Matter Research, New York University, New York, NY 10003

A tractor beam is a travelling wave that transports illuminated objects back to its source, opposite to the wave's direction of propagation, along its entire length. The requisite retrograde force arises when an object scatters the wave's momentum density downstream into the direction of propagation, and then recoils upstream by conservation of momentum. Achieving this condition imposes constraints on the structure of the wave, which we elucidate in the Rayleigh limit, when the wavelength exceeds the size of the object. Continuously propagation-invariant modes such Bessel beams do not satisfy these conditions at dipole order in the multipole expansion, and so cannot serve as general-purpose long-ranged tractor beams. Modes with discrete propagation invariance, however, can act as first-order tractor beams. We demonstrate this by introducing a class of minimal solenoidal waves together with a set of design criteria that distinguish tractor beams that pull objects from repulsor beams that push them.

I. INTRODUCTION

Radiation pressure commonly is understood to push illuminated objects downstream along the direction of light's propagation. The recent realization [1–4] that appropriately structured traveling waves can pull objects upstream consequently has excited considerable interest. Retrograde forces arise when an illuminated object scatters more of the wave's momentum into the downstream direction than otherwise would have been present [5–7]. The object then recoils upstream to conserve momentum. This happens, for example, when a small particle enters the diverging wave downstream of the focus in an optical trap, redirects light into the forward direction, and then recoils toward the focus [5–7]. The trapping beam's divergence, however, inherently limits how far it can pull an object upstream.

Achieving long-range retrograde transport requires a non-diffracting or weakly-diffracting mode. A plane wave cannot serve in this capacity because all of its momentum is directed along the axis of propagation. Remarkably enough, some other non-diffracting traveling waves [1–4, 8] have the requisite characteristics. Such modes have come to be known as tractor beams because of their resemblance to the popular science fiction trope [9].

Previously identified tractor-beam modes were discovered empirically [1, 2, 8]. Few have been demonstrated experimentally [2, 8, 10], and most of these demonstrations have relied on fine tuning of material properties [8, 10]. Here, we present an analytical theory for optical tractor beams that applies in the simplifying, yet practically important limit that the transported object is smaller than the wavelength of light, the so-called Rayleigh regime. This theoretical framework expresses the forces experienced by an illuminated object in terms of the experimentally controllable amplitude and phase profiles of a vector mode of light. It reveals that the most commonly discussed tractor-beam mode [1, 3, 4, 11] is inherently undermined by its continuous propagation invariance; such beams can pull only under exceptional circumstances, and then only weakly. These drawbacks can be avoided by creating tractor beams from modes that display *discrete* propagation invariance. We illustrate this by introducing a family of minimal solenoidal tractor-beam modes that exert retrograde forces as first-order photokinetic effects.

II. PHOTOKINETIC FORCES

The electric and magnetic fields in a monochromatic beam of light at frequency ω may be projected into Cartesian components,

$$\boldsymbol{E}(\boldsymbol{r},t) = \sum_{j=1}^{3} E_j(\boldsymbol{r})\, e^{-i\omega t}\, \hat{\epsilon}_j \quad \text{and} \tag{1a}$$

$$\boldsymbol{B}(\boldsymbol{r},t) = -\frac{i}{\omega}\, \nabla \times \boldsymbol{E}(\boldsymbol{r},t) \tag{1b}$$

$$= \sum_{j=1}^{3} B_j(\boldsymbol{r})\, e^{-i\omega t}\, \hat{\epsilon}_j, \tag{1c}$$

where $E_j(\boldsymbol{r})$ and $B_j(\boldsymbol{r})$ are the complex-valued electric and magnetic field amplitudes along the Cartesian coordinate $\hat{\epsilon}_j$. For comparison with experimental implementations, it is convenient to express these field components in terms of real-valued amplitudes and phases,

$$E_j(\boldsymbol{r}) = u_j(\boldsymbol{r})\, e^{i\phi_j(\boldsymbol{r})}, \tag{2}$$

and similarly for $B_j(\boldsymbol{r})$. Expressing optical forces in terms of $u_j(\boldsymbol{r})$ and $\phi_j(\boldsymbol{r})$ yields insights that are useful for designing and optimizing beams of light for optical micromanipulation, including tractor beams.

A. First-order photokinetic forces

Photokinetic forces arise from light's ability to polarize small objects. For simplicity and clarity, we will confine our discussion to optically isotropic objects whose dimensions are small enough relative to the wavelength of light

that they may be treated as point-like scatterers. In this so-called Rayleigh regime, the light's leading-order effect is to induce electric and magnetic dipole moments,

$$\boldsymbol{p}(\boldsymbol{r},t) = \alpha_e \boldsymbol{E}(\boldsymbol{r},t) \quad \text{and} \tag{3a}$$
$$\boldsymbol{m}(\boldsymbol{r},t) = \alpha_m \boldsymbol{B}(\boldsymbol{r},t), \tag{3b}$$

respectively, where α_e and α_m are the object's electric and magnetic dipole polarizabilities.

The induced dipole moments described by Eq. (3) experience time-averaged forces in gradients of the electric [12] and magnetic [13] fields,

$$\boldsymbol{F}_e(\boldsymbol{r}) = \frac{1}{2}\,\Re\left\{\sum_{j=1}^{3} p_j(\boldsymbol{r},t)\nabla E_j^*(\boldsymbol{r},t)\right\} \quad \text{and} \tag{4a}$$
$$\boldsymbol{F}_m(\boldsymbol{r}) = \frac{1}{2}\,\Re\left\{\sum_{j=1}^{3} m_j(\boldsymbol{r},t)\nabla B_j^*(\boldsymbol{r},t)\right\}. \tag{4b}$$

Although Eq. (4) completely describes optical dipole forces, how to control these forces is more clearly revealed when they are presented in terms of the amplitudes and the phase of the fields. Expressed in these terms, the electric dipole force has the form [14, 15]

$$\boldsymbol{F}_e(\boldsymbol{r}) = \frac{1}{4}\,\alpha_e'\nabla\sum_{j=1}^{3} u_j^2(\boldsymbol{r}) + \frac{1}{2}\,\alpha_e''\sum_{j=1}^{3} u_j^2(\boldsymbol{r})\nabla\phi_j(\boldsymbol{r}), \tag{5}$$

where α_e' and α_e'' are the real and imaginary parts of α_e, respectively.

Equation (5) and the analogous expression for the magnetic dipole force constitute the first-order photokinetic forces. The first term on the right-hand side of Eq. (5) describes the manifestly conservative intensity-gradient force responsible for trapping by single-beam optical traps such as optical tweezers [5]. The second describes a non-conservative contribution to radiation pressure that is directed by gradients of the phase [14, 16, 17]. Recognizing that these phase gradients define the local wave vector [18] and that α_e'' and α_m'' are positive for conventional materials, the phase-gradient term tends to drive objects downstream along the beam of light.

Light's polarization plays remarkably little role in first-order photokinetic effects. This can be appreciated because phase differences among the Cartesian components that determine the degree of circular polarization are absent from Eq. (5). Even so, polarization-dependent photokinetic effects are well documented in the experimental literature [19–21] and emerge naturally in numerical studies [19, 22–24]. Such effects can be attributed to higher-order photokinetic forces.

B. Higher-order photokinetic forces

Higher-order photokinetic effects result both from forces exerted on higher-order induced multipoles and also from interference between different types and orders of multipole scattering [3]. The multipole polarizabilities that parametrize these higher-order terms generally become rapidly smaller with increasing multipole order, particularly for objects that are smaller than the wavelength of light. For Rayleigh particles, the leading-order corrections to the first-order dipole forces arise from the interference between the scattered electric and magnetic dipole fields, and from the induced electric quadrupole moment. The dipole-interference term in particular provides a mechanism for creating propagation-invariant tractor beams.

Dipole scattering by a small isotropic particle gives rise to a second-order force of the form [3, 13]

$$\boldsymbol{F}_{em}(\boldsymbol{r}) = -\frac{k^4}{12\pi\epsilon_0 c}\,\Re\left\{\alpha_e\alpha_m^*\boldsymbol{E}(\boldsymbol{r},t)\times\boldsymbol{B}^*(\boldsymbol{r},t)\right\}. \tag{6}$$

Expressing this in terms of the fields' amplitudes and phases yields four distinctive contributions,

$$\boldsymbol{F}_{em}(\boldsymbol{r}) = \frac{\epsilon k^3}{24\pi\epsilon_0}\,\Im\left\{\alpha_e\alpha_m^*\right\}\,\nabla\sum_{j=1}^{3} u_j^2(\boldsymbol{r}) \tag{7a}$$
$$-\frac{\epsilon k^3}{12\pi\epsilon_0}\,\Re\left\{\alpha_e\alpha_m^*\right\}\sum_{j=1}^{3} u_j^2(\boldsymbol{r})\nabla\phi_j(\boldsymbol{r}) \tag{7b}$$
$$-\frac{\epsilon k^3}{12\pi\epsilon_0}\,\Re\left\{\alpha_e\alpha_m^*\right\}\,\nabla\cdot\mathsf{T}^{(a)}(\boldsymbol{r}) \tag{7c}$$
$$-\frac{\epsilon k^3}{12\pi\epsilon_0}\,\Im\left\{\alpha_e\alpha_m^*\right\}\nabla\cdot\mathsf{T}^{(s)}(\boldsymbol{r}), \tag{7d}$$

where ϵ is the permeability of the medium and where we have introduced the antisymmetric (a) and symmetric (s) components of the Maxwell stress tensor,

$$T_{ij}^{(a)}(\boldsymbol{r}) = u_i(\boldsymbol{r})u_j(\boldsymbol{r})\,\sin\bigl(\phi_j(\boldsymbol{r})-\phi_i(\boldsymbol{r})\bigr) \quad \text{and} \tag{8a}$$
$$T_{ij}^{(s)}(\boldsymbol{r}) = u_i(\boldsymbol{r})u_j(\boldsymbol{r})\,\cos\bigl(\phi_j(\boldsymbol{r})-\phi_i(\boldsymbol{r})\bigr). \tag{8b}$$

Equation (7) is the complete result for the dipole-interference contribution, including both electric and magnetic contributions. The force it describes tends to be weaker than the first-order dipole force described by Eq. (5) because $k^3\,|\alpha_e| \ll 1$ in the Rayleigh regime. Even so, each term in Eq. (7) has interesting implications for optical micromanipulation.

The intensity-gradient term in Eq. (7a) either strengthens or weakens the first-order trapping force depending on material parameters that affect the sign of $\Im\{\alpha_e\alpha_m^*\}$. Because $\Re\{\alpha_e\alpha_m^*\} \gtrless 0$ for conventional materials, the phase-gradient term in Eq. (7b) describes a retrograde force that could provide the basis for a tractor beam were it not generally weaker than the first-order phase-gradient term from Eq. (5).

Equations (7c) and (7d) describe optical forces with properties distinct from those of dipole forces, and thus create new avenues for optical micromanipulation. We can interpret Eq. (7c) by noting that

$$\boldsymbol{s}(\boldsymbol{r}) = \frac{\epsilon}{2\omega}\Im\left\{\boldsymbol{E}^*(\boldsymbol{r},t)\times\boldsymbol{E}(\boldsymbol{r},t)\right\} \tag{9a}$$

is the time-averaged spin angular momentum density carried by the beam of light [18, 25–27]. From this, we obtain the general result,

$$\nabla \cdot \mathsf{T}^{(a)}(\boldsymbol{r}) = \frac{\omega}{\epsilon} \nabla \times \boldsymbol{s}(\boldsymbol{r}), \tag{9b}$$

which identifies Eq. (7c) as a force arising from the curl of the spin angular momentum density in a nonuniform beam of light [21]. Spin-curl forces have been a subject of active research [15, 21, 27–31] and here may be identified as a second-order photokinetic effect. They may be directed along the axis of propagation, and thus can contribute to the retrograde forces in a tractor beam.

The remaining term in Eq. (7d) describes a complementary curl-free force field directed along the local axis of linear polarization. This term also can give rise to a retrograde force in longitudinally polarized traveling waves of the kind observed in experiments on crossed plane waves [8].

Induced-quadrupole contributions to the optical force also arise at second order in the multipole expansion and so may be comparable in strength to the dipole-interference force. This contribution has the form [3]

$$\boldsymbol{F}_q(\boldsymbol{r}) = \frac{1}{4}\Re\left\{\sum_{j,k} Q_{jk}(\boldsymbol{r},t)\nabla\partial_j E_k^*(\boldsymbol{r},t)\right\}, \tag{10}$$

where the induced quadrupole moment is

$$Q_{jk}(\boldsymbol{r},t) = \frac{1}{2}\gamma_e\left[\partial_j E_k(\boldsymbol{r},t) + \partial_k E_j(\boldsymbol{r},t)\right] \tag{11}$$

for a neutral particle with scalar quadrupole susceptibility, γ_e. The induced-quadrupole force is symmetric under exchange of the Cartesian components of $\boldsymbol{E}(\boldsymbol{r},t)$. Consequently, it does not depend on the spin angular momentum of the light, and does not contribute to spin-dependent photokinetic effects.

Second-order forces are weaker than first-order forces for Rayleigh particles. Higher multipole contributions will be weaker still. We will focus, therefore, on identifying characteristics of propagation-invariant modes of light that are useful for creating first-order tractor beams.

III. PROPAGATION-INVARIANT TRACTOR BEAMS

Achieving long-ranged retrograde transport without active intervention [32] requires a tractor beam to be based on a weakly-diffracting or propagation-invariant mode. Ideally, such a mode would carry retrograde momentum [33] along its entire length, and thus exert retrograde radiation pressure. It is sufficient, however, for the axial component of the beam's momentum density to be smaller than the plane-wave limit. In that case, an illuminated particle can scatter additional momentum downstream, and thus recoil upstream. The archetype for such a tractor beam is the Bessel beam [34–37], which originally was proposed for this application in the context of acoustic waves [1].

Bessel beams can be generated from the longitudinal vector potential

$$\boldsymbol{A}_{m,\alpha}(\boldsymbol{r}) = u_{m,\alpha}\, A_{m,\alpha}(\boldsymbol{r})\hat{z}, \quad \text{where} \tag{12a}$$

$$A_{m,\alpha}(\boldsymbol{r}) = J_m(kr\sin\alpha)\, e^{im\theta}\, e^{ikz\cos\alpha} \tag{12b}$$

is the scalar cylindrical harmonic that is characterized by convergence angle α and an integer winding number m. The overall amplitude, $u_{m,\alpha}$, sets the intensity of the beam. Equation (12) is expressed in cylindrical coordinates, $\boldsymbol{r} = (\rho,\theta,z)$, aligned with the propagation direction, $\hat{z}$. The fields in a Bessel beam may be obtained from $\boldsymbol{A}_{m,\alpha}(\boldsymbol{r})$ as [34, 35]

$$\boldsymbol{E}^{\mathrm{TE}}_{m,\alpha}(\boldsymbol{r},t) = \nabla \times \boldsymbol{A}_{m,\alpha}(\boldsymbol{r})\, e^{-i\omega t}, \tag{13}$$

with the magnetic field following from Eq. (1b). Equation (13) describes a transverse electric (TE) Bessel beam that is equivalent to the form presented in [3]. The corresponding transverse magnetic (TM) mode can be obtained by exchanging the electric and magnetic fields in Eq. (13). Bessel beams with more general polarizations may be obtained as linear superpositions of these TE and TM modes. The range of non-diffracting propagation is proportional to $\csc\alpha$, and so is longer for beams with smaller convergence angles, α [37, 38].

Because the Bessel beams form a complete orthogonal basis, any propagation-invariant mode can be expressed as a linear superposition of Bessel beams. Those superpositions comprising Bessel beams with the same convergence angle, α, display continuous propagation invariance. Any such non-diffracting beam lacks axial intensity gradients as a matter of definition, so that $\partial_z u^2(\boldsymbol{r}) = 0$. The remaining phase-gradient contribution to the axial dipole force is purely repulsive for any material with $\alpha_e'' > 0$ and $\alpha_m'' > 0$. From this, we conclude that **no continuously propagation-invariant beam of light can serve as a general-purpose first-order tractor beam**.

Non-diffracting modes nonetheless may act as tractor beams for particles whose scattering properties favor retrograde forces from higher-order contributions [3]. To illustrate this, we consider the photokinetic force exerted by TE Bessel beams and contrast this with the performance of TM Bessel beams. The axial component of the force then has the form

$$\boldsymbol{F}(\boldsymbol{r})\cdot\hat{z} = \frac{1}{2}k\,u_{m,\alpha}^2\frac{J_m^2(kr\sin\alpha)}{r^2}\cos\alpha\, f(\alpha,x), \tag{14}$$

where $x = kr\sin\alpha$ and where $f(\alpha,x)$ is a polarization-dependent factor describing the particle's coupling to the light. The axial force vanishes in the strongly converging limit because the Bessel beam becomes a standing wave at $\alpha = \pi/2$.

The coupling factor for a TE-polarized Bessel beam due to dipole and dipole-interference contributions is

$$f^{\mathrm{TE}}(\alpha,x)=g_m^2(x)\left(\alpha_e''+\alpha_m''-\frac{\epsilon k^3}{6\pi\epsilon_0}\Re\left\{\alpha_e\alpha_m^*\right\}\right)+\sin^2\alpha\left[x^2-g_m^2(x)\right]\alpha_m'', \quad (15)$$

with the mode-dependent geometric factor

$$g_m^2(x)=m^2+x^2\frac{{J_m'}^2(x)}{{J_m}^2(x)}. \quad (16)$$

The equivalent expression for TM modes is obtained by transposing α_e and α_m.

The electric and magnetic quadrupole contributions to the axial force are strictly repulsive, with the electric quadrupole repulsion being somewhat weaker in TM-polarized modes. Quadrupole contributions therefore do not help to create a second-order tractor beam.

Considering, for the moment, only those contributions to the axial force arising from dipole terms, the direction of motion depends on the sign of $f^{\mathrm{TE}}(\alpha,x)$, and therefore on the particle's position within the beam. Retrograde forces appear at positions x that satisfy

$$\frac{g_m^2(x)}{x^2}<\frac{\sin^2\alpha\,\alpha_m''}{\frac{\epsilon k^3}{6\pi\epsilon_0}\Re\left\{\alpha_e\alpha_m^*\right\}-\alpha_e''-\cos^2\alpha\,\alpha_m''}. \quad (17)$$

The absence of solutions in the limit of small α demonstrates that weakly converging Bessel beams generally act as repulsors. More strongly converging modes can act as tractor beams if the radial component of the force vanishes at positions that satisfy Eq. (17). This occurs, for example, in TE modes with $m=\pm1$ along the principal intensity maximum at $r=0$. Such beams can stably pull an object upstream if the convergence angle satisfies

$$\sin^2\alpha>1+\frac{\alpha_e''}{\alpha_m''}-\frac{\epsilon k^3}{6\pi\epsilon_0}\left(\alpha_e''+\alpha_e'\frac{\alpha_m'}{\alpha_m''}\right). \quad (18)$$

Because Eq. (17) neglects the quadrupole contribution, it constitutes a necessary condition for a Bessel beam to act as a second-order tractor beam, but is not a sufficient condition.

Numerical studies involving all orders of multipole scattering confirm that Bessel beams can act as tractor beams for some objects that are larger than the wavelength of light [3, 4, 11]. The present considerations demonstrate that the necessary pulling force does not arise at first order, but rather emerges from a competition between first-order repulsion and higher-order retrograde forces. Because such tractor beams require comparatively steep convergence angles, moreover, they do not lend themselves to long-range transport.

IV. FIRST-ORDER SOLENOIDAL TRACTOR BEAMS

Relaxing the condition of continuous propagation invariance in favor of discrete propagation invariance,

$$u^2(r,\theta,z+\Delta z)=u^2(r,\theta,z), \quad (19)$$

creates opportunities for strong, long-ranged, general-purpose tractor beams that operate at first order. Axial intensity gradients in a discretely propagation invariant beam can establish retrograde forces that counteract repulsive phase-gradient forces. This is the principle by which an optical conveyor establishes an axial array of traps [32]. Achieving continuous retrograde transport in such a beam requires a continuous path through the beam along which the net optical force acts in the retrograde direction. Optical conveyors do not have this property, but waves displaying screw invariance can. These include spiral waves [39] and solenoidal beams [2]. Although solenoidal waves have been described and their efficacy as tractor beams has been demonstrated experimentally [2], the nature of their force fields has not been explored previously. Applying the theory of photokinetic effects reveals that solenoidal modes can act as first-order tractor beams.

Discretely propagation-invariant beams can be created by superposing two mutually coherent Bessel beams with different convergence angles. Because we are interested in long-range transport, we choose component Bessel beams with small convergence angles, which may be described in the paraxial approximation as TEM modes with uniform polarization, $\hat{\epsilon}$. The superposition then has the form

$$\boldsymbol{E}(\boldsymbol{r},t)=\left[u_{m,\alpha}A_{m,\alpha}(\boldsymbol{r},t)+u_{n,\beta}A_{n,\beta}(\boldsymbol{r},t)\right]\hat{\epsilon}. \quad (20)$$

The resulting axial interference pattern is spatially periodic, as required, and stationary. Superposing modes with the same winding number creates optical conveyors [32, 40, 41]. Superposing modes with different winding numbers creates a solenoidal wave. We will order the contributions with $|m|>|n|$. The original description of solenoidal waves [2] involved superpositions of large numbers of Bessel modes. Being composed of just two modes, the solenoidal waves presented here may be considered minimal realizations of the genus.

We ensure that a solenoidal mode traps particles at a radius $r=R$ by choosing the convergence angles α and β so that extremum p of mode m overlaps extremum q of mode n. This condition ensures $\partial_r\left|\boldsymbol{E}(\boldsymbol{r},t)\right|^2=0$ along $r=R$. Equation (5) then ensures that $\hat{r}\cdot\boldsymbol{F}_e(\boldsymbol{r})|_{r=R}=0$. The intensity maximum at $r=R$ acts as a potential energy well along the radial direction for light-seeking particles with $\alpha_e'>0$. It is achieved by setting

$$\frac{\sin\alpha}{j_{m,p}'}=\frac{\sin\beta}{j_{n,q}'}=\frac{1}{kR}, \quad (21)$$

where $x=j_{m,p}'$ is the p-th root of $J_m'(x)=0$.

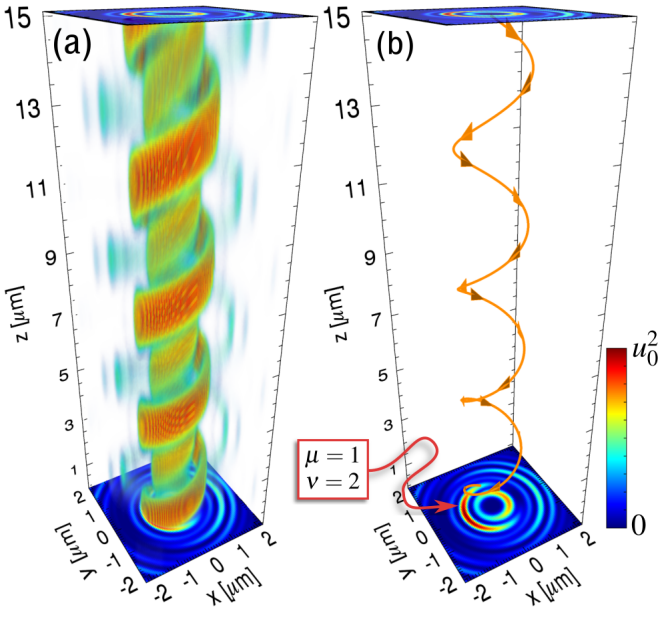

FIG. 1. (color online) (a) Calculated intensity distribution of a right-handed solenoidal tractor beam with a vacuum wavelength of 532 nm and design parameters $m = -5$ and $n = -4$, $\alpha = 0.418$ rad and $\beta = 0.627$ rad, propagating along $+\hat{z}$ through water. (b) Computed trajectory of a 50 nm-diameter silica sphere moving along the tractor beam in (a). The color bar indicates the local intensity, $u^2(\boldsymbol{r})$.

Interference is optimized if the two components contribute equally to the amplitude, u_0, at $r = R$. This establishes a relationship between the amplitudes

$$u_{\alpha,m} J_m(j'_{m,p}) = u_{\beta,n} J_n(j'_{n,q}) = \frac{1}{2} u_0. \tag{22}$$

The resulting superposition has the form

$$\boldsymbol{E}(\boldsymbol{r}, t) = u(\boldsymbol{r})\, e^{i\phi(\boldsymbol{r})} e^{-i\omega t} \hat{x}, \tag{23a}$$

with amplitude and phase profiles along $r = R$ of

$$u(\boldsymbol{r})|_{r=R} = u_0 \cos\left(\frac{m-n}{2} \left[\theta - 2\pi \frac{z}{\Delta z} \right] \right) \quad \text{and} \tag{23b}$$

$$\phi(\boldsymbol{r})|_{r=R} = \ell\theta + \frac{\cos\alpha + \cos\beta}{2} kz. \tag{23c}$$

This is a helical mode that carries orbital angular momentum [42] proportional to its winding number,

$$\ell = \frac{m+n}{2}. \tag{23d}$$

The axial pitch of the solenoid's spiraling intensity distribution is

$$\Delta z = \frac{2\pi}{k} \frac{m-n}{\cos\alpha - \cos\beta}. \tag{23e}$$

Interestingly, solenoidal waves with half-integer winding numbers do not differ qualitatively from those with integer winding numbers. The 2ℓ-fold sign changes in $u(\boldsymbol{r})$, as defined in Eq. (23b), eliminate the transverse vortices that otherwise would form in a helical beam with non-integer winding number [43, 44].

The transverse intensity distribution is proportional to $u^2(\boldsymbol{r})$ and has a number of maxima equal to $|m-n|$. These maxima spiral once around $\hat{z}$ each time the axial position z advances by Δz. The spiral is right-handed for positive values of Δz.

For simplicity, we will consider this wave's influence on dielectric Rayleigh particles, for which the electric dipole force described by Eq. (5) dominates the magnetic dipole force and all other multipole contributions. We then define the locus, $\boldsymbol{r}_s(z) = (R, \theta_s, z)$, of the solenoidal trap to be the set of points along which intensity-gradient forces compensate the axial component of the radiation pressure, $F_z(\boldsymbol{r}_s) = 0$. This condition is satisfied along the spiral curve

$$\theta_s(z) = 2\pi \frac{z}{\Delta z} + \theta_0, \tag{24a}$$

with angular offset,

$$\theta_0 = \frac{2}{m-n} \tan^{-1}\left(\frac{\alpha''_e}{\alpha'_e} \frac{\cos\alpha + \cos\beta}{\cos\alpha - \cos\beta} \right). \tag{24b}$$

The path that a particular object takes through the beam runs parallel to this. Such solutions exist for small objects regardless of the light-scattering properties encoded in α_e. Whether or not these solutions act as traps depends on whether or not the particle also is stably trapped in the radial direction. Small dielectric particles are stably trapped along the bright locus described by Eq. (23); reflecting and absorbing particles might not be.

A solenoidal trap acts as a tractor beam if the azimuthal component of the radiation pressure, $F_\theta(\boldsymbol{r}_s)$, drives the trapped particle into a region where the axial component of the force, $F_z(\boldsymbol{r}_s)$, points in the retrograde direction, $F_\theta(\boldsymbol{r}_s)\ \partial_\theta F_z(\boldsymbol{r})|_{\boldsymbol{r}=\boldsymbol{r}_s} < 0$. This condition is satisfied if

$$n\cos\alpha > m\cos\beta. \tag{25}$$

Flipping the sense of this inequality transforms a tractor beam into a repulsor that pushes objects downstream rather than pulling them upstream.

Equation (25) is the principal design requirement for creating a general-purpose first-order tractor beam. With this constraint, Eq. (21) then requires $q > p$. Minimizing α and β to maximize pulling range then requires $q = p + 1$. Maximizing the pulling force by maximizing the intensity along the solenoid's principal spiral then yields $p = 1$ and $q = 2$ as optimal choices.

Equations (21), (22) and (25) constitute previously lacking design criteria for general-purpose first-order tractor beams. As described, they establish conditions on the individual Bessel components' convergence angles, α and β, and winding numbers, m and n. Equivalently,

these conditions may be expressed in terms of the radius, R, pitch, Δz, winding number, ℓ, and non-diffracting range of the desired tractor beam. Previously, functional solutions had to be sought numerically [2].

The example of a solenoidal tractor beam presented in Fig. 1(a) was designed according to these principles. Figure 1(b) shows the computed trajectory of a 50 nm-diameter silica sphere moving through water in its force field. Because solenoidal tractor beams operate at dipole order, they should be inherently stronger than higher-order tractor beams based on continuously invariant modes.

Accounting for the magnetic field's contribution to the optical force shifts θ_0 by an amount that depends on the relative magnitudes of α_e and α_m. The net effect is to strengthen the pulling force, at least for conventional materials.

Polarization also can enhance a solenoidal tractor beam's performance. For example, Eq. (7c) shows that a solenoid beam created with right-circularly polarized light has a transverse spin-curl force of the form

$$\boldsymbol{F}_{\mathrm{sc}}(\boldsymbol{r}) = \frac{\epsilon k^3}{24\pi\epsilon_0}(\alpha_e'\alpha_m' + \alpha_e''\alpha_m'')\left(\frac{\hat{r}}{r}\partial_\theta - \hat{\theta}\partial_r\right)u^2(\boldsymbol{r}). \tag{26}$$

When applied to a right-handed solenoidal tractor beam, this increases $F_\theta(r)$ for $r < R$ and decreases it for $r > R$. By moderating the trapped particle's speed in this way, $\boldsymbol{F}_{\mathrm{sc}}(\boldsymbol{r})$ contributes to a kinematic trap that tends to localize an object near $r = R$ as it is transported by the beam.

V. DISCUSSION

The two-component solenoidal tractor beams described here illustrate the process by which first-order tractor beams may be designed and optimized using the theory of photokinetic effects. More sophisticated superpositions [2] may have superior properties, but at the cost of additional complexity. For some applications, solenoidal waves based on other helical modes, such as Laguerre-Gaussian beams, may be preferable.

Beyond its immediate application to designing tractor beams, the theory of photokinetic effects offers additional benefits for optical micromanipulation. Expressing optical forces in terms of experimentally accessible quantities helps to elucidate the origin of experimentally observed phenomena. The polarization-dependent contribution from Eq. (7d), for example, explains why linearly polarized optical tweezers exert anisotropic in-plane forces [16, 23]. The circulation of optically isotropic spheres in circularly polarized optical tweezers similarly may be identified with the spin-curl force from Eq. (7c). Polarization-dependent size selectivity in the force created by crossed plane waves [8] can be explained as arising from competition between the phase-gradient terms in Eq. (5) and Eq. (7b). Such observations provide guidance for designing and optimizing new modes of optical micromanipulation, including tractor beams.

The development presented here directly addresses the forces experienced by objects that are substantially smaller than the wavelength of light. For larger particles, the forces described by Eqs. (5) and (7) are augmented and possibly dominated by higher-order multipole contributions. For Rayleigh particles, we expect the first-order forces described by Eq. (5) to be substantially stronger than any higher-order contributions, including those described by Eq. (7). Applying these considerations to the particular case of tractor beams, we conclude that Bessel beams generally push small objects whereas appropriately designed solenoidal waves can pull them.

ACKNOWLEDGMENTS

This work was supported by the National Science Foundation under Grant No. DMR-1305875. AY acknowledges support from a NASA Space Technology Research Fellowship under Award No. NNX15AQ40H.

[1] Philip L. Marston, "Axial radiation force of a Bessel beam on a sphere and direction reversal of the force," J. Acoust. Soc. Am. **120**, 3518–3524 (2006).
[2] Sang-Hyuk Lee, Yohai Roichman, and David G. Grier, "Optical solenoid beams," Opt. Express **18**, 6988–6993 (2010).
[3] Jun Chen, Jack Ng, Zhifang Lin, and C. T. Chan, "Optical pulling force," Nature Photonics **5**, 531–534 (2011).
[4] Andrey Novitsky, Cheng-Wei Qiu, and Haifeng Wang, "Single gradientless light beam drags particles as tractor beams," Phys. Rev. Lett. **107**, 203601 (2011).
[5] A. Ashkin, J. M. Dziedzic, J. E. Bjorkholm, and S. Chu, "Observation of a single-beam gradient force optical trap for dielectric particles," Opt. Lett. **11**, 288–290 (1986).
[6] Art Ashkin, "Forces of a single-beam gradient laser trap on a dielectric sphere in the ray optics regime," Biophys. J. **61**, 569–582 (1992).
[7] A. Ashkin, "Optical trapping and manipulation of neutral particles using lasers," Proc. Natl. Acad. Sci. U.S.A. **94**, 4853–4860 (1997), review of optical tweezer applications by the father of the field.
[8] O. Brzobohatý, V. Karásek, M. Šiler, L. Chvátal, T. Čižmár, and P. Zemánek, "Experimental demonstration of optical transport, sorting and self-arrangement using a 'tractor beam'," Nature Photonics **7**, 123–127 (2013).
[9] Edward E. Smith, "Spacehounds of IPC," Amazing Stories **6**, 1–100 (1931).
[10] Vladlen Shvedov, Arthur R. Davoyan, Cyril Hnatovsky, Nader Engheta, and Wieslaw Krolikowski, "A long-range polarization-controlled optical tractor beam," Nature Phot. **8**, 846–850 (2014).

[11] Andrey Novitsky, Cheng-Wei Qiu, and Andrei Lavrinenko, "Material-independent and size-independent tractor beams for dipole objects," Phys. Rev. Lett. **109**, 023902 (2012).

[12] P. C. Chaumet and M. Nieto-Vesperinas, "Time-averaged total force on a dipolar sphere in an electromagnetic field," Opt. Lett. **25**, 1065–1067 (2000).

[13] Patrick C. Chaumet and Adel Rahmani, "Electromagnetic force and torque on magnetic and negative-index scatterers," Opt. Express **17**, 2224–2234 (2009).

[14] Yohai Roichman, Bo Sun, Yael Roichman, Jesse Amato-Grill, and David G. Grier, "Optical forces arising from phase gradients," Phys. Rev. Lett. **100**, 013602 (2008), arXiv:cond-mat/0703543 [cond-mat.soft].

[15] David B. Ruffner and David G. Grier, "Comment on 'Scattering forces from the curl of the spin angular momentum of a light field'," Phys. Rev. Lett. **111**, 059301 (2013).

[16] Yohai Roichman, Bo Sun, Allan Stolarski, and David G. Grier, "Influence of non-conservative optical forces on the dynamics of optically trapped colloidal spheres: The fountain of probability," Phys. Rev. Lett. **101**, 128301 (2008), arXiv:0804.0730.

[17] P. Y. Wu, R. X. Huang, C. Tischer, A. Jonas, and E. L. Florin, "Direct measurement of the nonconservative force field generated by optical tweezers," Phys. Rev. Lett. **103**, 108101 (2009).

[18] M. V. Berry, "Optical currents," J. Opt. A **11**, 094001 (2009).

[19] A. Rohrbach, "Stiffness of optical traps: Quantitative agreement between experiments and electromagnetic theory," Phys. Rev. Lett. **95**, 168102 (2005).

[20] Ebrahim Madadi, Akbar Samadi, Mojtaba Cheraghian, and Nader S. Reihani, "Polarization-induced stiffness asymmetry of optical tweezers," Opt. Lett. **37**, 3519–3521 (2012).

[21] David B. Ruffner and David G. Grier, "Optical forces and torques in non-uniform beams of light," Phys. Rev. Lett. **108**, 173602 (2012).

[22] A. R. Zahkarian, P. Polynkin, M. Mansuripur, and J. V. Moloney, "Single-beam trapping of micro-beads in polarized light: Numerical simulations," Opt. Express **14**, 3660–3676 (2006).

[23] R. S. Dutra, N. B. Viana, P. A. Maia Neto, and H. M. Nussenzveig, "Polarization effects in optical tweezers," J. Opt. A **9**, S221–S227 (2007).

[24] Bo Sun, Yohai Roichman, and David G. Grier, "Theory of holographic optical trapping," Opt. Express **16**, 15765–15776 (2008).

[25] M. V. Berry and M. R. Dennis, "Polarization singularities in isotropic random vector waves," Proc. Royal Soc. A **457**, 141–155 (2001).

[26] Aleksandr Bekshaev, Konstantin Y. Bliokh, and Marat Soskin, "Internal flows and energy circulation in light beams," J. Opt. **13**, 053001 (2011).

[27] Konstantin Bliokh, Justin Dressel, and Franco Nori, "Conservation of the spin and orbital angular momentum in electromagnetism," New J. Phys. **16**, 093037 (2014).

[28] N. B. Simpson, K. Dholakia, L. Allen, and M. J. Padgett, "Mechanical equivalence of spin and orbital angular momentum of light: An optical spanner," Opt. Lett. **22**, 52–54 (1997).

[29] Silvia Albaladejo, Manuel I. Marqués, Marine Laroche, and Juan José Sáenz, "Scattering forces from the curl of the spin angular momentum," Phys. Rev. Lett. **102**, 113602 (2009).

[30] X. L. Wang, J. Chen, Y. Li, J. Ding, C. S. Guo, and H. T. Wang, "Optical orbital angular momentum from the curl of polarization," Phys. Rev. Lett. **105**, 253602 (2010).

[31] A. Ya. Bekshaev, "Subwavelength particles in an inhomogeneous light field: optical forces associated with the spin and orbital energy flows," J. Opt. **15**, 044004 (2013).

[32] David B. Ruffner and David G. Grier, "Optical conveyors: A class of active tractor beams," Phys. Rev. Lett. **109**, 163903 (2012).

[33] M. V. Berry, "Quantum backflow, negative kinetic energy, and optical retro-propagation," J. Phys. A **43**, 415302 (2010).

[34] Xuesong Zhou, "Normal and abnormal vector wave functions and their conversion relations," Scientia Sinica **27**, 1226–1232 (1984).

[35] Zdeněk Bouchal and Marek Olvik, "Non-diffractive vector Bessel beams," J. Mod. Opt. **42**, 1555–1566 (1995).

[36] J. Durnin, "Exact-solutions for nondiffracting beams. 1. the scalar theory," J. Opt. Soc. Am. A **4**, 651–654 (1987).

[37] J. Durnin, J. J. Miceli, Jr, and J. H. Eberly, "Diffraction-free beams," Phys. Rev. Lett. **58**, 1499–1501 (1987).

[38] J. Arlt, V. Garcés-Chávez, W. Sibbett, and K. Dholakia, "Optical micromanipulation using a Bessel light beam," Opt. Commun. **197**, 239–245 (2001), a zeroth-order Bessel light beam focuses to a non-diffracting line of light useful for aligning rods and creating stacks of particles. Creates stacks of up to 9 5 μm sphers and transports 1 μm spheres over 1 mm.

[39] S. Chávez-Cerda, G. S. McDonald, and G. H. C. New, "Nondiffracting beams: travelling, standing, rotating and spiral waves," Opt. Commun. **123**, 225–233 (1996).

[40] Tomáš Čižmar, Veneranda Garcés-Chávez, Kishan Dhokalia, and Pavel Zemánek, "Optical conveyor belt for delivery of submicron objects," Appl. Phys. Lett. **86**, 174101 (2005).

[41] David B. Ruffner and David G. Grier, "Universal, strong and long-ranged trapping by optical conveyors," Opt. Express **22**, 26834–26853 (2014).

[42] L. Allen, M. W. Beijersbergen, R. J. C. Spreeuw, and J. P. Woerdman, "Orbital angular-momentum of light and the transformation of Laguerre-Gaussian laser modes," Phys. Rev. A **45**, 8185–8189 (1992).

[43] M. V. Berry, "Optical vortices evolving from helicoidal integer and fractional phase steps," J. Opt. A **6**, 259–269 (2004).

[44] Jonathan Leach, Eric Yao, and Miles J. Padgett, "Observation of the vortex structure of a non-integer vortex beam," New J. Phys. **6**, 71 (2004).